Hyperfine splittings and Zeeman infrared absorption of Tb^{3+}-doped CaF_2 and SrF_2

Jon-Paul R. Wells* and Glynn D. Jones
Department of Physics and Astronomy, University of Canterbury, PB4800, Christchurch 8020, New Zealand
(Received 9 June 2009; published 4 September 2009)

We report on the observation of pseudoquadrupole splittings of sharp infrared-absorption lines of $CaF_2:Tb^{3+}$. These splittings are large enough to be directly observed because the Tb^{3+} electronic ground levels consists of two singlets separated by only 0.18 cm^{-1} for the F^- C_{4v} center. Both the hyperfine splittings and measured Zeeman splittings for F^- C_{4v} centers in $CaF_2:Tb^{3+}$ and $SrF_2:Tb^{3+}$ can be accounted for using wave functions derived from a previously published crystal-field analysis of experimental energy levels.

DOI: 10.1103/PhysRevB.80.115105 PACS number(s): 71.70.Ch

I. INTRODUCTION

Alkaline-earth fluoride crystals (CaF_2, SrF_2, and BaF_2) have received widespread attention from spectroscopists as model systems for the study of clustering kinetics or defect chemistry, particularly for doping with trivalent rare-earth ions. In the early sixties, relatively comprehensive electron-paramagnetic-resonance (EPR) studies mapped out the site distribution for low to medium concentrations of trivalent rare earths (RE^{3+}) via spectroscopy of the ground state.[1] With the advent in the midseventies of laser selective excitation (lse),[2] optical techniques were able to contribute in a substantiative manner and, in particular, the defect distribution of non-Kramers, ions which are usually inaccessible to EPR, could be determined. The major center in $CaF_2:RE^{3+}$ crystals is a C_{4v} symmetry RE^{3+}-F^- pair, with a charge compensating F^- ion occupying an interstitial nearest-neighbor position along the $\langle 100\rangle$ direction from the RE^{3+} ion.[3–14] The CaF_2 and SrF_2 hosts differ in that, for RE^{3+} ions beyond Ho^{3+} in SrF_2, the principal center has C_{3v} symmetry with a charge compensating interstitial fluorine ion located in the next-nearest-neighbor position along the $\langle 111\rangle$ direction. By contrast, the major center in BaF_2 has trigonal C_{3v} symmetry throughout the RE^{3+} series.[10,15]

Quantum computer hardware is under development utilizing various approaches from all-optical techniques to a variety of solid-state designs. Recently, the hyperfine structure of rare-earth ions has received attention because of the possibility of its utilization as hardware for quantum information processing.[16–19] As suggested in Ref. 18, it is the manufacturing capabilities of the solid-state industries which may more readily lend these systems to scalability of the particular computational scheme. Seen in this context, rare-earth-doped crystals have the attractive feature that they have shielded $4f$ valence shells and therefore sharp atomiclike line spectra. The quantum information would be stored in the nuclear states of these ions, which have coherence times that can be many tens of milliseconds.

Our previous work on Ho^{3+} (Ref. 20) demonstrated complex hyperfine patterns for absorption transitions to the $^5I_7$ multiplet of $CaF_2:Ho^{3+}$ including relaxation of the ΔI_z selection rule through wave-function mixing via the perpendicular hyperfine interaction. Here we report infrared-absorption studies of $CaF_2:Tb^{3+}$ and $SrF_2:Tb^{3+}$. The regular Tb^{3+}, F^- C_{4v} centers in both CaF_2 and SrF_2 crystals are unusual in that they have a low-lying first-excited (γ_4) singlet level whose energy is less than 0.5 cm^{-1} above that of the singlet (γ_3) ground level. This gives rise to the possibility of measuring the hyperfine structure of Tb^{3+} directly in an absorption measurement through a large enhancement of the pseudoquadrupole interaction between these levels. Zeeman infrared-absorption studies of the sharp Tb^{3+} spectral lines of these centers show measurable splittings due to the nonlinear Zeeman interaction between the ground and first-excited-state singlets as well as Zeeman splittings of upper-state doublets. The Zeeman splittings of all the Tb^{3+} levels can be readily accounted for by magnetic field calculations using wave functions derived from previously published crystal-field analyses.[11] High-resolution scans of these lines appear to show Tb^{3+} hyperfine structure due to the 100% abundant ^{159}Tb isotope with a nuclear spin I of $\frac{3}{2}$. Such structure is rarely reported for the Tb^{3+} ions in an optical experiment.[21]

Orbital singlet levels are not usually considered to have an associated magnetic moment. However for close-lying singlet levels, as reported here, an effective moment is obtained through J_z interactions such as the Zeeman interaction and the pseudoquadrupole hyperfine interaction.[22] This can be thought of as arising because the electronic angular momentum operator J_z transforms as a γ_2 under C_{4v} symmetry and as such couples the $Z_1\gamma_3$ and $Z_2\gamma_4$ ground and first-excited levels of the F^-C_{4v} centers of Tb^{3+} in both CaF_2 and SrF_2.

II. EXPERIMENT

CaF_2 and SrF_2 crystals containing between 0.005–0.1 molar % of TbF_3 were grown by the temperature-gradient (Bridgman-Stockbarger) technique in a 38 kW Arthur D. Little R.F. furnace. Appropriate amounts of the relevant alkaline-earth fluoride and TbF_3 were placed in a graphite crucible and then lowered at approximately 4 mm hr^{-1} through the temperature gradient provided by the induction coils of the rf furnace. Excellent optical-quality crystals up to 4 cm in length could be obtained. Oriented samples were obtained from these boules through alignment via their (111) cleavage planes.

Infrared-absorption spectra were measured using a Bio-Rad FTS-40 Fourier transform infrared spectrometer (FTIR) for the 1800–4500 cm^{-1} region appropriate to the $^7F_6 \rightarrow {}^7F_5$, $^7F_4$, and $^7F_3$ transitions of the Tb^{3+} ion. The samples

were mounted on a copper holder and cooled by thermal contact with the 10 K stage of a CTI LTS 0.1 closed cycle helium cryostat.

Zeeman spectra were measured with a 4T Oxford Instruments superconducting solenoid built into the can of a liquid-helium cryostat. The infrared beam was directed along a hollow tube fixed through the center of the solenoid. The crystals were cooled by thermal contact with a copper sample holder, whose screw fitted into the middle of this tube. As the magnet is a simple solenoid, infrared Zeeman measurements could only be made along the direction of the magnetic field. Although not directly relevant here, this will restrict observations to allowed transitions for the $\mathbf{B}\|\mathbf{k}$ polarization geometry. The magnet homogeneity is 1% over the central 1 cm volume while sample thicknesses up to 3 cm were required to observe the weak Tb^{3+} transitions. 0.04 cm^{-1} resolution scans were performed on the infrared-absorption lines of the $CaF_2:Tb^{3+}$ and $SrF_2:Tb^{3+}$ samples using the Bomem DA3.02 FTIR spectrometer at New Zealand Industrial Research limited in Wellington.

III. INFRARED SPECTROSCOPY OF $CaF_2:Tb^{3+}$ and $SrF_2:Tb^{3+}$

A. 0.25 cm^{-1} infrared-absorption spectra

Infrared-absorption measurements have been made on long $CaF_2:0.07\%Tb^{3+}$ and $SrF_2:0.09\%Tb^{3+}$ crystals cooled to 10 K. Figures 1 and 2 show infrared-absorption transitions to the $^7F_5$, $^7F_4$, and $^7F_3$ multiplets for 2.5-cm-long crystals. The transitions observed in Figs. 1 and 2 are assigned by comparison with laser selective excitation measurements[11] which allow transitions of the F^- C_{4v} center to be unambiguously identified. The remaining unmarked transitions are attributed to other Tb^{3+} centers (F^- C_{3v} and cluster centers) not identified by lse as well as atmospheric absorption water and CO_2 lines. We focus our attention on the F^- C_{4v} center.

The spectroscopy of these F^- C_{4v} centers is unusual because of the proximity of the first-excited state ($Z_2\gamma_4$) to the ground state ($Z_1\gamma_3$), of 0.18 and 0.48 cm^{-1} for CaF_2 and SrF_2, respectively.[23,24] This leads to a substantial first-excited-state population even at 10 K and we expect transitions to be observable from both the ground and first-excited state. However, these close transitions could not be resolved at the maximum resolution of 0.1 cm^{-1} of the Digilab FTIR spectrometer. Selection rules[25] for transitions from these singlet levels only allow transitions to excited levels transforming as either γ_3 or γ_4 orbital singlets or as γ_5 doublets. Transitions to either γ_1 or γ_2 singlet levels are not present in the infrared-absorption spectra. Transitions to the lowest levels of a given upper multiplet yield the sharpest lines as the higher levels of a given multiplet are able to undergo intra-multiplet relaxation via the spontaneous emission of appropriate lattice phonons, even at 10 K. In both hosts, the transition to the $X_2\gamma_4$ level is among the sharpest lines of those measured because the lowest $X_1\gamma_1$ level is less than 22 cm^{-1} lower in energy.[11] Direct relaxation is improbable because such low energies are not readily supported by the lattice. Table I lists the measured energies as determined from infrared absorption.

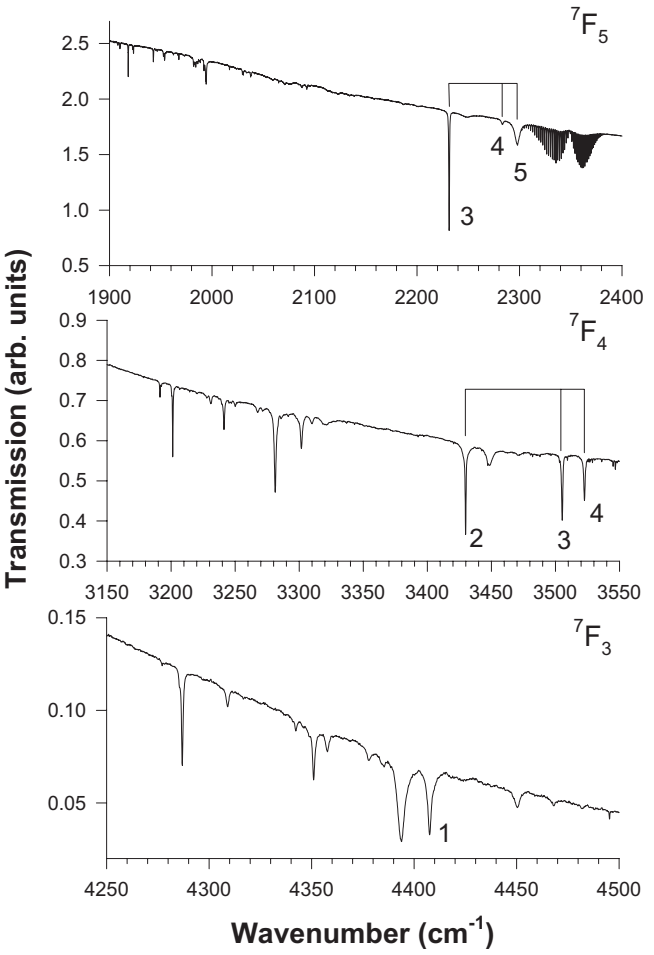

FIG. 1. 10 K infrared-absorption spectra for transitions to the $^7F_5$, $^7F_4$, and $^7F_3$ multiplets of $CaF_2:0.07\%Tb^{3+}$. The lines indicate F^- C_{4v} center transitions whose upper multiplet states are labeled by the appropriate numerical subscript for various levels of the given upper multiplet.

B. Zeeman infrared-absorption spectra

⟨111⟩ Zeeman infrared-absorption spectra were recorded at 0.1 cm^{-1} resolution. For a magnetic field directed along a (111) crystal direction, all C_{4v} centers are magnetically equivalent and the Tb^{3+} site symmetry is reduced to C_1. All of the observed F^- C_{4v} center transitions to the $^7F_5$, $^7F_4$, and $^7F_3$ multiplets showed a common ground-state splitting (as shown in Figs. 3 and 4), with an $s_{\langle 111\rangle}$ splitting factor of 9.87 ± 0.10 and 10.18 ± 0.10 for CaF_2 and SrF_2, respectively, (see Table II). As the $s_\|$ and $s_{\langle 111\rangle}$ splitting factors are related by $s_{\langle 111\rangle}=s_\|/\sqrt{3}$ (with $s_\perp=0$) these values correspond to $s_\|$ splitting factors of 17.10 and 17.63, in general, agreement with the values derived from EPR (Refs. 23 and 24) of 17.77 ± 0.02 and 17.95 ± 0.05.

At magnetic fields above 2 T, transitions to the Y_3 and X_4 γ_5 doublets in CaF_2 and the Y_3, X_4, and W_2 doublets in SrF_2 also exhibit Zeeman splittings of their upper doublet levels. These Zeeman split components can only be observed for the transitions from the $Z_1\gamma_3$ ground level. For fields above 2 T the $Z_1\gamma_3$ and $Z_2\gamma_4$ levels have separated sufficiently that the $Z_2\gamma_4$ level is depopulated (by an order of magnitude) at 10 K

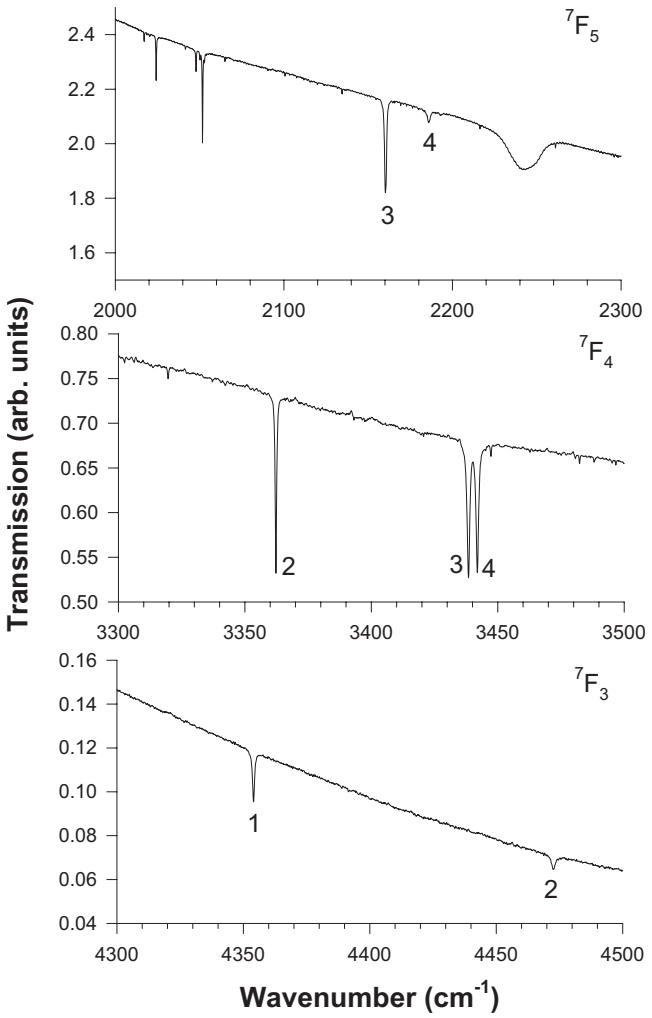

FIG. 2. 10 K infrared-absorption spectra for transitions to the $^7F_5$, $^7F_4$, and $^7F_3$ multiplets of SrF_2:0.09%Tb^{3+}. The F^- C_{4v} center transitions are labeled by the appropriate numerical subscript.

(Fig. 3 and 4). All of the derived magnetic splitting factors are listed in Table II.

TABLE I. Measured 10 K infrared-absorption lines (in vacuum cm^{-1}; ±0.10), intensities (relative to that of the strongest line set to 100; ±2), and linewidths (in cm^{-1}; ±0.1) for the F^- C_{4v} centers of CaF_2:0.07%Tb^{3+} and SrF_2:0.09%Tb^{3+}.

Energy level (C_{4v} irrep)		CaF_2			SrF_2		
		Energy	Intensity	Width	Energy	Intensity	Width
$^7F_5$	$Y_3(\gamma_5)$	2231.83	60	0.7	2160.65	82	1.1
	$Y_4(\gamma_3)$	2283.83	8	1.7	2186.08	16	1.6
	$Y_5(\gamma_5)$	2298.51	29	3.8			
$^7F_4$	$X_2(\gamma_4)$	3430.44	32	0.7	3362.54	69	0.5
	$X_3(\gamma_3)$	3506.04	67	0.9	3439.72	93	0.8
	$X_4(\gamma_5)$	3523.44	16	0.9	3442.34	84	0.8
$^7F_3$	$W_1(\gamma_3)$	4409.05	100	1.4	4354.54	54	0.6
	$W_2(\gamma_5)$				4473.52	100	1.1

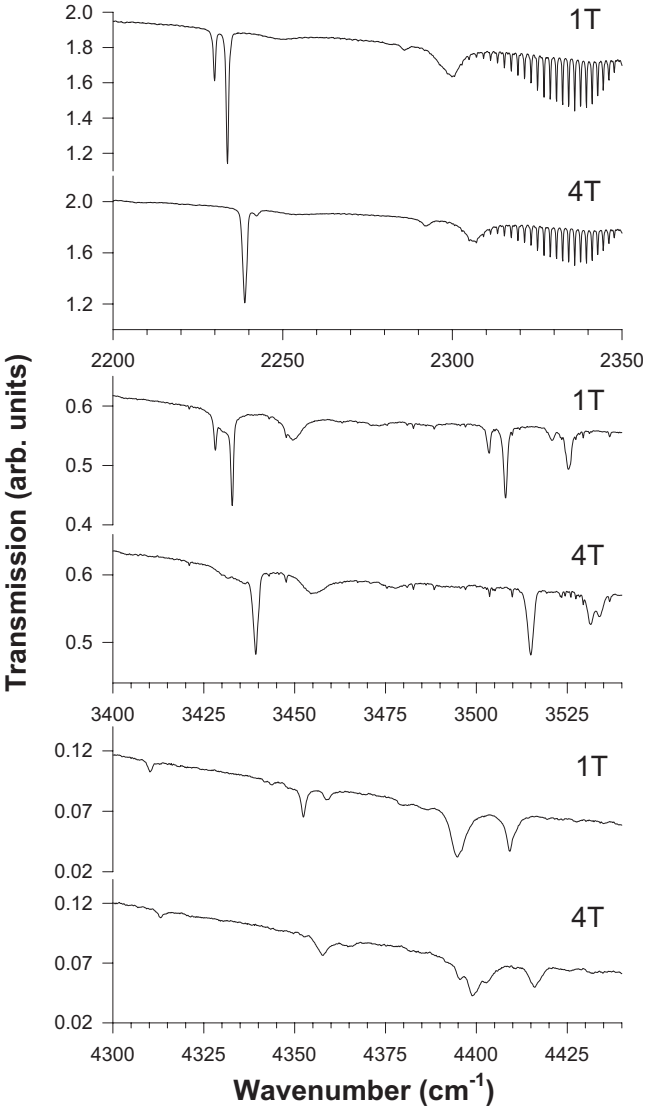

FIG. 3. ⟨111⟩ Zeeman infrared spectra for the F^- C_{4v} center in CaF_2:0.07%Tb^{3+}.

In order to account for the measured Zeeman splittings, the appropriate crystal and magnetic field matrices were simultaneously diagonalised. A standard Hamiltonian was used, of the form

$$H = H_{\text{freeion}} + H_{\text{cf}} + H_{\text{Zeeman}}.$$

The free-ion Hamiltonian H_{freeion} is

$$H_{\text{freeion}} = E_{\text{avg}} + \sum_k F^k f_k + \alpha L(L+1) + \beta G(G_2) + \gamma G(R_7) + \sum T^i t_i + \zeta_{\text{SO}} A_{\text{SO}} + \sum P^k p_k + \sum M^j m_j. \quad (1)$$

The crystal-field Hamiltonian H_{cf} appropriate for C_{4v} symmetry is

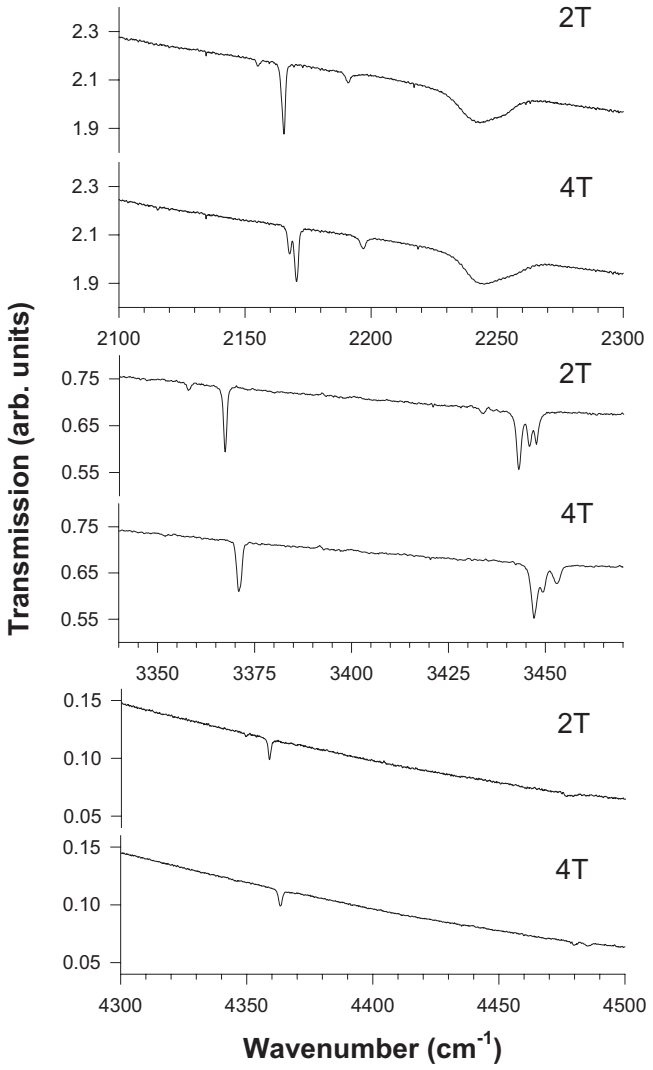

FIG. 4. ⟨111⟩ Zeeman infrared spectra for the F^- C_{4v} center in $SrF_2:0.09\%Tb^{3+}$.

$$H_{\rm cf} = B_A^2 C_0^{(2)} + B_A^4\left[C_0^{(4)} - \sqrt{\frac{7}{10}}(C_4^{(4)} + C_{-4}^{(4)})\right] + B_A^6\left[C_0^{(6)} + \sqrt{\frac{1}{14}}(C_4^{(6)} + C_{-4}^{(6)})\right] + B_C^4\left[C_0^{(4)} + \sqrt{\frac{5}{14}}(C_4^{(4)} + C_{-4}^{(4)})\right] + B_C^6\left[C_0^{(6)} - \sqrt{\frac{7}{2}}(C_4^{(6)} + C_{-4}^{(6)})\right] \quad (2)$$

TABLE II. Calculated and measured magnetic splitting factors (±0.10) for the F^- C_{4v} centers in $CaF_2:Tb^{3+}$ and $SrF_2:Tb^{3+}$. The magnetic field was applied in the ⟨111⟩ direction

State	Field (Tesla)	CaF_2 Calc	CaF_2 Expt.	SrF_2 Calc	SrF_2 Expt.
$Z_1(\gamma_{3,4})$	1	10.34	9.87	10.32	10.18
$Y_3(\gamma_5)$	4	2.33	1.84	1.31	1.42
$X_4(\gamma_5)$	4	1.36	1.30	1.82	1.88
$W_2(\gamma_5)$	4			2.6	2.8 ± 0.2

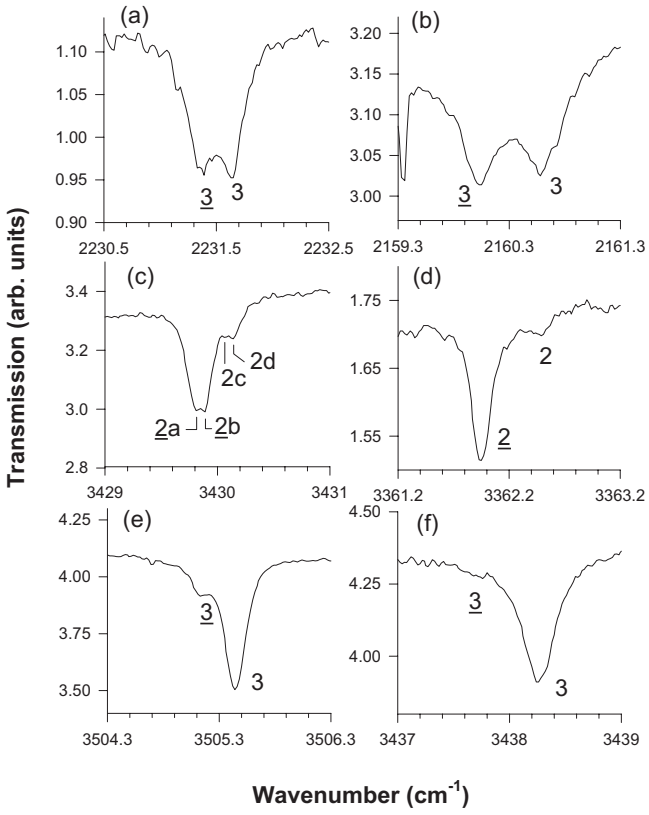

FIG. 5. 10 K, 0.04 cm^{-1} resolution, infrared-absorption transitions for $CaF_2:0.005\%Tb^{3+}$ and $SrF_2:0.01\%Tb^{3+}$: the $Y_3\gamma_5$ level for (a) CaF_2 and (b) SrF_2; the $X_2\gamma_4$ level for (c) CaF_2 and (d) SrF_2; the $X_3\gamma_3$ level for (e) CaF_2 and (f) SrF_2. For all figures, but (c), the underlined numeral denotes a transition from the $Z_2\gamma_4$ first-excited level whereas no underline denotes a transition from the $Z_1\gamma_3$ ground level. In (c) the notation refers to the labeling of levels given in Table IV.

with the experimental data from Ref. 11. refitted for our purposes. For Zeeman analyses, an interaction term

$$H_{\rm Zeeman} = \mu_B(\mathbf{L} + 2\mathbf{S}) \cdot \mathbf{B} \quad (3)$$

was added, where $\mu_B = 0.4669$ cm^{-1}/T is the Bohr magneton. The magnetic splitting factor for a particular level is defined by $s = \Delta E/\mu_B B$, where ΔE is the energy splitting in a magnetic field B. Excellent overall agreement is obtained as shown in Table II. This gives confidence that these crystal-field wave functions are a good set for analysis of the hyperfine structure.

C. High-resolution splittings and hyperfine structure

Figure 5 shows 0.04 cm^{-1} resolution infrared-absorption spectra for transitions to the $Y_3\gamma_5$, $X_2\gamma_4$, and $X_3\gamma_3$ levels of the F^- C_{4v} centers in $CaF_2:0.005\%Tb^{3+}$ and $SrF_2:0.01\%Tb^{3+}$ as measured at a nominal temperature of 10 K. For these states, this highest available resolution is sufficient to observe the close separation of the Tb^{3+} ground and first-excited states. The relative intensities of the split components confirm the state symmetry assignments made in Ref. 11 as $\gamma_3 \rightarrow \gamma_4$ and $\gamma_4 \rightarrow \gamma_3$ transitions should only be

TABLE III. Calculated magnetic hyperfine constants A_J (in GHz) and intermediate-coupled Lande g factors for multiplets of the Tb^{3+} ion. *A_J value measured for the $^7F_6$ ground multiplet (Ref. 26).

Multiplet	A_J	Lande g factor
$^7F_6$	0.530*	1.49
$^7F_5$	0.468	1.50
$^7F_4$	0.556	1.47
$^7F_3$	0.410	1.49
$^7F_2$	0.395	1.49
$^7F_1$	0.386	1.49
$^5D_4$	0.527	1.46

allowed through mixing of the ground-state wave functions via the pseudoquadrupole hyperfine interaction (and any small magnetic dipole transition moment which can only be expected for $^7F_6 \rightarrow {}^7F_5$). Thus a transition to an excited-state γ_5 doublet would be expected to show equal intensity components, a transition to an excited-state singlet transforming as a γ_3 irrep would show a stronger higher-energy component and a transitions to a γ_4 state would show a stronger intensity lower-energy component. This is clearly confirmed in the spectra displayed in Figs. 5(a)–5(f). A high-resolution spectrum was not measured for transitions to the $W_1\gamma_3$ state with the Bomem spectrometer.

Figure 5(c) shows a barely resolved splitting of 0.07 cm^{-1}, observed for $CaF_2:Tb^{3+}$, for each $Z_1\gamma_3$ and $Z_2\gamma_4$ component line. It is possible that these splittings arise from the pseudoquadrupole hyperfine interaction between the $I=\frac{3}{2}$ nuclear-spin states of the 100% abundant ^{159}Tb isotope and the $Z_1\gamma_3$ and $Z_2\gamma_4$ electronic ground states. These electronic states have wave functions of the form

$$Z_1\gamma_3{:}(0.7062)|6\rangle + (0.7062)|-6\rangle,$$

$$Z_2\gamma_4{:}(0.7068)|6\rangle - (0.7068)|-6\rangle$$

with $\langle\gamma_4|J_z|\gamma_3\rangle=5.98$. The $|\pm I_z\rangle$ hyperfine components of the ground-state levels are mixed by the hyperfine interaction $A_6I_zJ_z$ to yield a spectrum of energies corresponding to $\pm\sqrt{\Delta^2+[A_6I_zJ_z]^2}$. Here $2\Delta=0.18$ cm^{-1} and A_6, the magnetic hyperfine constant for the $^7F_6$ multiplet of Tb^{3+}, is 0.530 GHz.[26] The magnetic hyperfine constants for other Tb^{3+} multiplets have been calculated using Eq. 5.19 of Wybourne[27] in intermediate coupling

$$A_J = a_l\left\{2 - g + 2\left[\frac{12(2J+1)}{J(J+1)}\right]^{1/2}\langle f^N\alpha SL||V^{(12)}||f^N\alpha' S'L'\rangle \times \begin{pmatrix} S & S' & 1 \\ L & L' & 2 \\ J & J & 1 \end{pmatrix}\right\}, \quad (4)$$

where $a_l=2\mu_B\mu_N g_l\langle r^{-3}\rangle$, g_l is the nuclear g factor and g is the landé g factor corrected for intermediate coupling. These hyperfine constants are listed in Table III. Table IV shows the calculated and experimental splittings with good agreement between the two. Thus the measured line structure is consistent with the observation of pseudoquadrupole splittings arising from the closely spaced ground and first-excited states.

The $Y_3\gamma_5$ level at 2231.8 cm^{-1} has a comparable linewidth to the $X_3\gamma_3$ transition for which hyperfine splittings were observed. To estimate the magnitude of the hyperfine splittings for this level, consider the calculated electronic wave function

$$Y_3\gamma_5{:}-(0.4721)|\mp 3\rangle + (0.7153)|\pm 5\rangle + (0.4919)|\pm 1\rangle$$

with $\langle\gamma_5|J_z|\gamma_5\rangle=2.13$. For $A_5=0.468$ GHz (Table III) and with $E(I_z)=A_JI_zJ_z$ we obtain an evenly spaced pattern of four electron-nuclear levels each separated by 1 GHz. When this structure is superimposed on the pseudoquadrupole splittings between the ground and first-excited states, an overall spectrum of two groups of four lines are expected, each having an energy span of 4.3 GHz (or 0.14 cm^{-1}) separated by 5.3 GHz (for CaF_2). Thus the span of the expected splittings is

TABLE IV. Measured and calculated energies (in GHz; ±0.6) for hyperfine lines on the $Z_{1,2}(\gamma_{3,4})\rightarrow X_2\gamma_4$ transition of the F^- C_{4v} center in $CaF_2:Tb^{3+}$. E_0 is an arbitrarily chosen reference energy.

		Hyperfine Energy	
Hyperfine Line	Assigned Transition	Measured	Calculated
d	$\|Z_1\gamma_3\pm\frac{3}{2}\rangle\rightarrow\|X_2\gamma_4\rangle$	$E_0+2.34$	$E_0+2.16$
c	$\|Z_1\gamma_3\pm\frac{1}{2}\rangle\rightarrow\|X_2\gamma_4\rangle$	E_0	E_0
b	$\|Z_2\gamma_4\pm\frac{1}{2}\rangle\rightarrow\|X_2\gamma_4\rangle$	$E_0-6.26$	$E_0-5.52$
a	$\|Z_2\gamma_4\pm\frac{3}{2}\rangle\rightarrow\|X_2\gamma_4\rangle$	$E_0-8.60$	$E_0-7.56$

TABLE V. Nuclear wave-function composition $|I_z\rangle$ for the $Z_{1,2}(\gamma_{3,4})$ ground and first-excited states of the F^- C_{4v} center in $CaF_2:Tb^{3+}$ and $SrF_2:Tb^{3+}$.

	Wave function	
State	CaF_2	SrF_2
$Z_1(\gamma_3)\pm\frac{3}{2}$	$-0.8641\|\gamma_3\pm\frac{3}{2}\rangle\pm0.5033\|\gamma_4\pm\frac{3}{2}\rangle$	$-0.9579\|\gamma_3\pm\frac{3}{2}\rangle\pm0.2873\|\gamma_4\pm\frac{3}{2}\rangle$
$Z_1(\gamma_3)\pm\frac{1}{2}$	$-0.9649\|\gamma_3\pm\frac{1}{2}\rangle\pm0.2625\|\gamma_4\pm\frac{1}{2}\rangle$	$-0.9942\|\gamma_3\pm\frac{1}{2}\rangle\pm0.1079\|\gamma_4\pm\frac{1}{2}\rangle$
$Z_2(\gamma_4)\pm\frac{1}{2}$	$0.9649\|\gamma_4\pm\frac{1}{2}\rangle\pm0.2625\|\gamma_3\pm\frac{1}{2}\rangle$	$0.9942\|\gamma_4\pm\frac{1}{2}\rangle\pm0.1079\|\gamma_3\pm\frac{1}{2}\rangle$
$Z_2(\gamma_4)\pm\frac{3}{2}$	$0.8641\|\gamma_4\pm\frac{3}{2}\rangle\pm0.5033\|\gamma_3\pm\frac{3}{2}\rangle$	$0.9579\|\gamma_4\pm\frac{3}{2}\rangle\pm0.2873\|\gamma_3\pm\frac{3}{2}\rangle$

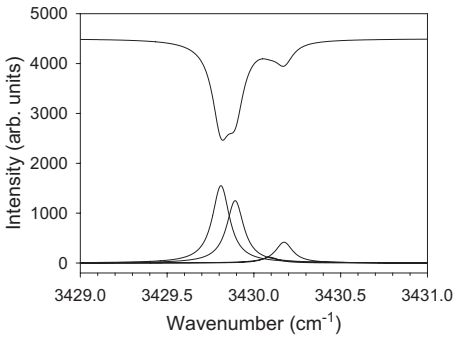

FIG. 6. Simulated 10 K absorption spectrum for transitions to the $X_2\gamma_4$ level in $CaF_2:Tb^{3+}$.

comparable to the separation between the electronic states and this is borne out in Fig. 5(a) although no distinct hyperfine splittings were resolved.

Figure 5(d) shows the $X_2\gamma_3$ transitions for the F^- C_{4v} center in $SrF_2:Tb^{3+}$. In contrast to $CaF_2:Tb^{3+}$, no hyperfine splittings are observable. This is attributed to the larger ground-state splitting of $2\Delta=0.48$ cm^{-1} for the F^- C_{4v} center in $SrF_2:Tb^{3+}$ which gives rise to a calculated pseudoquadrupole span of only 1.2 GHz (0.04 cm^{-1}); too small to be resolved. Table V shows the calculated electron-nuclear wave functions for the ground levels for both materials with 50% less wave-function mixing for SrF_2, which is also evident from the relative intensities of the CaF_2 and SrF_2 $Z_1\gamma_3 \rightarrow \gamma_4$ and $Z_2\gamma_4 \rightarrow \gamma_3$ infrared transitions.

Figure 6 shows a simulated spectrum for the transitions to the $X_2\gamma_4$ level in CaF_2. Following Martin *et al.*,[22] we write the transition intensities as

$$|\gamma_3 I_z\rangle \rightarrow |\gamma_4 I_z\rangle I(I_z) \propto |a_1(I_z)M + a_2(I_z)N|^2 \exp\left[\frac{-\Delta E(I_z)}{k_B T}\right],$$

$$|\gamma_4 I_z\rangle \rightarrow |\gamma_4 I_z\rangle I(I_z) \propto |a_3(I_z)N + a_4(I_z)M|^2 \exp\left[\frac{-\Delta E(I_z)}{k_B T}\right],$$

where a_{1-4} are the admixture coefficients of the electron-nuclear wave functions given in Table V, $\Delta E(I_z)$ are the calculated hyperfine splittings given in Table IV, k_B is Boltzmann's constant, and M and N are the dipole matrix elements between the ground and first-excited states and the X_{γ_4} level. Here we assume that the magnetic dipole matrix elements connecting the $Z_1\gamma_3$ ground level and the $X_2\gamma_4$ level are zero (i.e., $M=0$). This is justifiable because the ΔJ selection rules for magnetic dipole transitions are not upheld and our calculations indicate that crystal-field J mixing is negligible for this state. The relative intensities of the ΔI_z conserving transitions between the hyperfine levels shown in Fig. 6 are in broad agreement with the experimental data. The relative intensities are determined by the wave-function mixture induced by the pseudoquadrupole interaction.

IV. CONCLUSIONS

High-resolution scans of infrared-absorption lines of trivalent terbium in CaF_2 and SrF_2 crystals reveal fine structure due to close-lying electronic ground states. For the $Z_{1,2}\gamma_{3,4} \rightarrow X_2\gamma_4$ transitions of the F^- C_{4v} center of CaF_2, 0.07 cm^{-1} splitting is observed on each line component. Both the magnitude of the energy splittings and the relative intensities of the transitions are consistent with the observation of hyperfine structure due to a pseudoquadrupole interaction between the close-lying ground-level singlets. Such behavior is not observed for the analogous transition in SrF_2 crystals due to the larger ground-level separation. A crystal-field analysis yields wave functions which account well for these observations and for the measured Zeeman splittings.

ACKNOWLEDGMENTS

Thanks are due to M. Staines and R.G. Buckley of New Zealand Industrial Research Ltd. for use of their Bomem DA3.02 FTIR spectrometer as well as Mike Reid of the University of Canterbury for the use of his crystal-field fitting routines.

*Corresponding author; jon-paul.wells@canterbury.ac.nz

[1] See, for example, M. J. Weber and R. W. Bierig, Phys. Rev. **134**, A1492 (1964).
[2] D. R. Tallant and J. C. Wright, J. Chem. Phys. **63**, 2074 (1975).
[3] C. A. Freeth and G. D. Jones, J. Phys. C **15**, 6833 (1982).
[4] A. A. Antipin, I. N. Kurkin, G. K. Chirkin, and L. Ya. Shekun, Sov. Phys. Solid State **6**, 1590 (1965).
[5] R. J. Reeves, G. D. Jones, and R. W. G. Syme, Phys. Rev. B **46**, 5939 (1992).
[6] Jon-Paul R. Wells, G. D. Jones, and R. J. Reeves, Phys. Rev. B **60**, 851 (1999).
[7] A. A. Antipin, I. I. Kurkin, L. D. Livanova, I. Z. Potvorova, and L. Ya. Shekun, Sov. Phys. Solid State **11**, 821 (1966).
[8] Jon-Paul R. Wells and R. J. Reeves, Phys. Rev. B **61**, 13593 (2000).
[9] R. J. Hamers, J. R. Wietfeldt, and J. C. Wright, J. Chem. Phys. **77**, 683 (1982).
[10] J.-P. R. Wells and R. J. Reeves, Phys. Rev. B **64**, 035102 (2001).
[11] K. M. Murdoch, G. D. Jones, and R. W. G. Syme, Phys. Rev. B **56**, 1254 (1997).
[12] M. Mujaji, G. D. Jones, and R. W. G. Syme, Phys. Rev. B **46**, 14398 (1992).
[13] N. J. Cockroft, G. D. Jones, and R. W. G. Syme, J. Chem. Phys. **92**, 2166 (1990).
[14] N. M. Strickland and G. D. Jones, Phys. Rev. B **56**, 10916 (1997).

[15] J.-P. R. Wells, T. Dean, and R. J. Reeves, J. Lumin. **96**, 239 (2002).
[16] M. Nilsson, L. Rippe, N. Ohlsson, and S. Kröll, Phys. Scr., T **102**, 178 (2002).
[17] J. J. Longdell and M. J. Sellars, Phys. Rev. A **69**, 032307 (2004).
[18] L. Rippe, M. Nilsson, S. Kröll, R. Klieber and D. Suter, Phys. Rev. A **71**, 062328 (2005).
[19] O. Guillot-Nöel, Ph. Goldner, E. Antic-Fidancev, and J. L. Le Gouët, Phys. Rev. B **71**, 174409 (2005).
[20] J.-P. R. Wells, G. D. Jones, M. F. Reid, M. N. Popova, and E. P. Chukalina, Mol. Phys. **102**, 1367 (2004).
[21] G. K. Liu, J. Huang, R. L. Cone, and B. Jacquier, Phys. Rev. B **38**, 11061 (1988).
[22] J. P. D. Martin, T. Boonyarith, N. B. Manson, M. Mujaji, and G. D. Jones, J. Phys.: Condens. Matter **5**, 1333 (1993).
[23] P. A. Forrester and C. F. Hempstead, Phys. Rev. **126**, 923 (1962).
[24] A. A. Antipin, L. D. Livanova, and L. Ya. Shekun, Sov. Phys. Solid State **10**, 1025 (1968).
[25] G. F. Koster, J. O. Dimmock, R. G. Wheeler, and H. Statz, *Properties of the Thirty Two Point Groups* (MIT., Massachusetts, 1963).
[26] A. Abragam and B. Bleaney, *Electron Paramagnetic Resonance of Transition Ions* (Oxford University, New York, 1970).
[27] B. G. Wybourne, *Spectroscopic Properties of Rare Earths* (Interscience, New York, 1965).